◆ Human Brain Mapping 33:2843–2855 (2012) ◆

Modeling Conflict and Error in the Medial Frontal Cortex

Andrew R. Mayer,[1,2]* Terri M. Teshiba,[1] Alexandre R. Franco,[3] Josef Ling,[1] Matthew S. Shane,[1] Julia M. Stephen,[1] and Rex E. Jung[1,4]

[1]*The Mind Research Network, Albuquerque, New Mexico*
[2]*Departments of Neurology and Psychology, University of New Mexico, Albuquerque*
[3]*Department of Psychiatry and Behavioral Sciences, Emory University School of Medicine, Atlanta, Georgia*
[4]*Department of Neurosurgery, University of New Mexico School of Medicine, Albuquerque, New Mexico*

Abstract: Despite intensive study, the role of the dorsal medial frontal cortex (dMFC) in error monitoring and conflict processing remains actively debated. The current experiment manipulated conflict type (stimulus conflict only or stimulus and response selection conflict) and utilized a novel modeling approach to isolate error and conflict variance during a multimodal numeric Stroop task. Specifically, hemodynamic response functions resulting from two statistical models that either included or isolated variance arising from relatively few error trials were directly contrasted. Twenty-four participants completed the task while undergoing event-related functional magnetic resonance imaging on a 1.5-Tesla scanner. Response times monotonically increased based on the presence of pure stimulus or stimulus and response selection conflict. Functional results indicated that dMFC activity was present during trials requiring response selection and inhibition of competing motor responses, but absent during trials involving pure stimulus conflict. A comparison of the different statistical models suggested that relatively few error trials contributed to a disproportionate amount of variance (i.e., activity) throughout the dMFC, but particularly within the rostral anterior cingulate gyrus (rACC). Finally, functional connectivity analyses indicated that an empirically derived seed in the dorsal ACC/pre-SMA exhibited strong connectivity (i.e., positive correlation) with prefrontal and inferior parietal cortex but was anti-correlated with the default-mode network. An empirically derived seed from the rACC exhibited the opposite pattern, suggesting that sub-regions of the dMFC exhibit different connectivity patterns with other large scale networks implicated in internal mentations such as daydreaming (default-mode) versus the execution of top-down attentional control (fronto-parietal). *Hum Brain Mapp 33:2843–2855, 2012.*

Key words: conflict; error; FMRI; multimodal; selective attention

Additional Supporting Information may be found in the online version of this article.

Contract grant sponsor: National Institutes of Health; Contract grant numbers: 1 R03 DA022435-01A1, R21-NS064464-01A1; Contract grant sponsor: National Center for Research Resources, Centers of Biomedical Research Excellence; Contract grant number: P20 RR021938.

*Correspondence to: Andrew R. Mayer, Ph.D., The Mind Research Network, Pete and Nancy Domenici Hall, 1101 Yale Blvd. NE, Albuquerque, NM 87106, USA. E-mail: amayer@mrn.org

Received for publication 21 July 2010; Revised 22 April 2011; Accepted 9 June 2011

DOI: 10.1002/hbm.21405

Published online 5 October 2011 in Wiley Online Library (wileyonlinelibrary.com).

INTRODUCTION

The parsing of relevant and irrelevant information from both unimodal [Stroop, 1935] and multi-sensory sources [Johnson and Zatorre, 2005; Macaluso and Driver, 2005] requires a high degree of cognitive control. Neuroimaging studies have revealed several structures, including the dorsal medial frontal cortex (dMFC), dorsolateral prefrontal cortex (DLPFC), anterior insula and inferior parietal lobes, that are commonly activated across a variety (e.g., Stroop, the go/no-go, the flanker, and Simon tasks) of cognitive control paradigms [Banich et al., 2000; Braver et al., 2003; Hester et al., 2004; Ridderinkhof et al., 2004; Roberts and Hall, 2008; van Veen et al., 2001]. Two prominent models posit a role for the dMFC in either conflict monitoring [Botvinick et al., 2001; Carter and van Veen, 2007; Carter et al., 1998], or in error detection and error-likelihood monitoring [Brown and Braver, 2005], and these roles remain actively debated [Aarts et al., 2008]. The current set of experiments systematically examined the putative roles through experimental manipulation, statistical modeling and functional connectivity analyses during a multimodal numeric Stroop task.

Considerable evidence suggests that the anterior cingulate gyrus (ACC) may be specifically involved in the monitoring of errors [Hester et al., 2004; Kiehl et al., 2000; Ullsperger and von Cramon, 2001] or in conditions within which the likelihood of errors is higher [Brown and Braver, 2005; but see Nieuwenhuis et al., 2007]. Electrophysiological studies first demonstrated a large-amplitude, negative waveform (error-related negativity; ERN) occurring 100 ms following an error response [Falkenstein et al., 1991; Luu et al., 2000], which was subsequently localized to the ACC [Dehaene et al., 1994; van Veen and Carter, 2002; Yeung et al., 2004]. Single subject lesion/electrophysiology data implicates both the rostral (rACC) and dorsal ACC (dACC) in error processing [Swick and Turken, 2002], with trial-by-trial electrophysiology measurements predicting the blood oxygen level dependent (BOLD) response in the rACC [Debener et al., 2005]. A more recent FMRI study disambiguated error processing on trials with high pre-response conflict compared to trials with no pre-response conflict and found that the ACC responded more selectively during the detection of erroneous motor responses rather than during pure response conflict [Wittfoth et al., 2008].

The conflict model suggests the dMFC becomes activated during the detection of any competing, or mutually incompatible, information [Botvinick et al., 2001; Carter and van Veen, 2007; Carter et al., 1998]. Electrophysiological activity in the ACC has been measured invasively during high conflict trials [Davis et al., 2005], and non-invasive electrophysiological measurements of error-related negativity are greater in the ACC during conditions of high response conflict compared to error monitoring [Gehring and Fencsik, 2001]. Additionally, the magnitude of ACC involvement has been shown to be dependent on the ratio of incongruent (high conflict) and congruent (low conflict) trials and the resultant changes in expectation [Carter et al., 2000], as well as on whether the previous trial was congruent or incongruent [Botvinick et al., 1999]. However, other studies suggest that the dMFC is only activated following motor conflict (i.e., competing responses) rather than during pure stimulus conflict [Liston et al., 2006; van Veen et al., 2004], a hypothesis that we further evaluated in the current design.

Specific dMFC regions may also respond to conflict detection (dACC/pre-SMA) compared to error (rACC) processing [Garavan et al., 2003; Menon et al., 2001; Ridderinkhof et al., 2004; Taylor et al., 2006; Ullsperger and von Cramon, 2001]. The conflict theory suggests that the ACC drives lateral prefrontal cortex activity during the exertion of top-down cognitive control [Botvinick et al., 2001; Carter and van Veen, 2007; Carter et al., 1998], and ACC activity predicts adjustments in behavior and DLPFC activation [Kerns et al., 2004]. Other work suggests that activity in the default-mode network can be used to predict behavioral errors several seconds in advance [Eichele et al., 2008]. Therefore, regions of the dMFC involved in cognitive control should putatively demonstrate increased functional connectivity with the lateral prefrontal cortex and inferior parietal lobules, heteromodal cortical areas which have been implicated in top-down attentional control [Cabeza and Nyberg, 2000]. In contrast, error-related dMFC regions may exhibit increased functional connectivity with the default-mode network, which becomes active during internal mentations (e.g., daydreaming) and may signal the likelihood of an upcoming error [Eichele et al., 2008].

Although a positive correlation exists between the degree of response conflict and the probability of errors (i.e., the more the conflict, the greater the likelihood of errors), even high conflict trials typically have a relatively low error rate in the majority of cognitive control experiments in healthy subjects. However, a low number of error trials render the explicit modeling of error variance challenging, as too few trials often produce unreliable statistical estimates of functional activation. Previous imaging studies have either degraded stimulus quality, decreased the allowable response time window (e.g., a speeded task) or increased the pre-potency of conflicting responses [Brown and Braver, 2005; Garavan et al., 2002, 2003; Lutcke and Frahm, 2008]. While these experimental manipulations increase the frequency of errors, they also decrease subjective awareness of stimulus properties, decrease subjects' ability to correctly perceive an error, and/or artificially accentuate differences between conflict and non-conflict trials [van Veen and Carter, 2002].

The current experiment adopted a novel approach in which statistical models that either incorporate or isolate variance associated with error trials were directly contrasted [Murphy and Garavan, 2004]. This approach is not dependent on a large number of error trials and provides an alternative methodology for examining the contribution of a relatively few error trials to the processing of conflicting and non-conflicting information. We examined the effects of different forms of conflict (pure stimulus versus

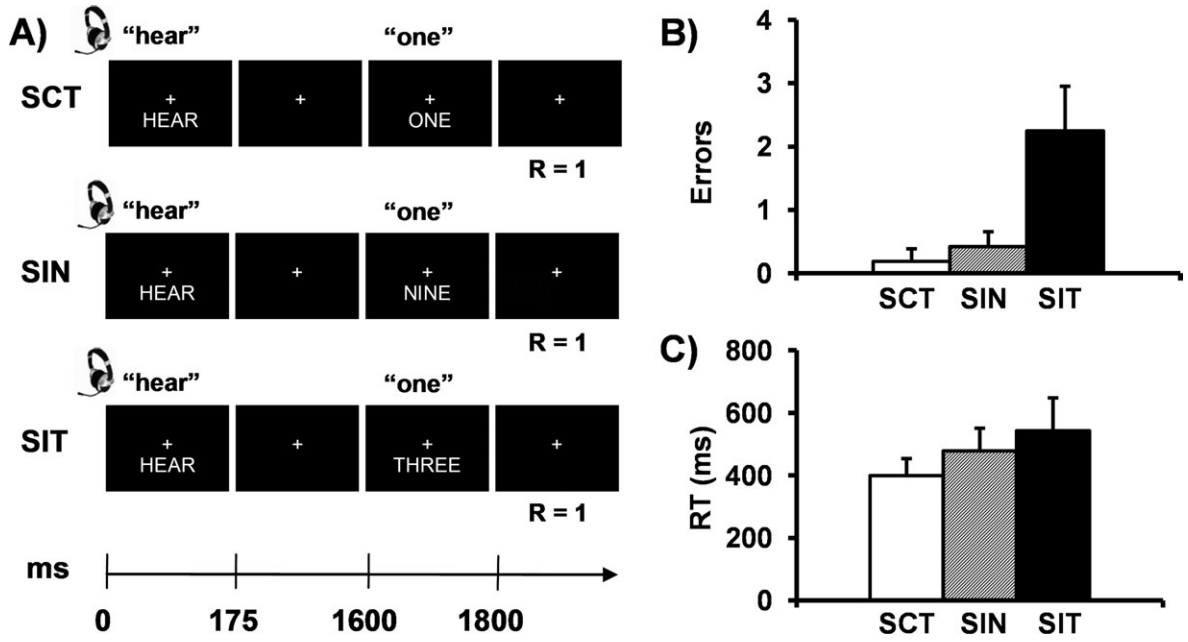

Figure 1.

Panel **A** presents a diagrammatic representation of the trial structure. "*R*" indicates the correct response for each condition illustrated. Panels **B** and **C** present the mean number of errors and median reaction times, respectively, for the congruent (SCT; white bar), incongruent with non-target distractor (SIN; gray bar), and incongruent with target distractor (SIT; black bar) conditions, collapsed across the auditory and visual modalities (error bars = 2 × standard error of the mean).

stimulus plus response selection) and error on dMFC activation during a multimodal numeric Stroop task (see Fig. 1A). Participants were presented with congruent multimodal numeric stimuli (low stimulus and response selection conflict; SCT trials), incongruent stimuli with a non-target distractor (medium stimulus and low response selection conflict; SIN trials) and incongruent stimuli with a target distractor (high stimulus and response selection conflict; SIT trials). The resulting hemodynamic response functions (HRF) for each trial were statistically modeled to either include [the untailored model; see Eq. (2)] or isolate [the tailored model; see Eq. (3)] the variance associated with error trials. The HRF from these models were then directly contrasted to determine the regions that showed differential hemodynamic responses based on the presence of error variance. The results from this contrast were then used as empirical seeds to determine the functional connectivity profile of various sub-regions of the dMFC and cortical networks implicated with top-down attentional control or error generation [Fox et al., 2005].

METHODS

Subjects

Twenty-six (13 males, 13 females) right-handed (mean Edinburgh Handedness Inventory score = 75.12% ± 23.37%) adult volunteers (mean age = 24.88 ± 4.70 years) completed the study. Of the 26 subjects, one subject was identified as an outlier (above three standard deviations) on task accuracy across several different trial types, and another subject exhibited difficulty understanding task instructions resulting in poor performance (above three standard deviations) on one trial type. These subjects were subsequently discarded from final analyses, leaving a final sample of 24 participants.

All participants completed a Symptom Checklist (SCL-90) to ensure that psychiatric history was negative for current symptoms including depression, anxiety, and other stress-related disorders known to affect neuropsychological performance on attention measures. None of the study participants were taking psychoactive medications or had a history of neurological, psychiatric or substance abuse disorders. Informed consent was obtained from all subjects according to institutional guidelines at the University of New Mexico.

Numeric Stroop Task

The general structure of trials was identical across all conditions and required participants to identify a target number (i.e., one, two, or three) by pressing a button as quickly and accurately as possible. A centrally-presented, white cross (visual angle = 1.41°) was presented on a

black background during the entire experiment to help participants maintain central fixation. The target number (exemplary visual angle = 9.73°) was preceded by a cue word (exemplary visual angle = 7.69°) indicating whether attention should be focused on one (selective attention conditions) or both sensory modalities (divided attention condition). The target number could be presented alone in one modality, or with an identical target number, a non-target distractor number, or a target distractor number in the opposite modality (see Fig. 1A). Cue and target durations were 175 and 200 ms, respectively. All visual stimuli were presented in word rather than Arabic form to maximize interference [Fias et al., 2001]. A 1,600 ms stimulus-onset asynchrony occurred between the presentation of the cue and target to permit the full allocation of attention resources.

In the selective attention conditions examining cognitive control, the word "HEAR" or "LOOK" was simultaneously presented in both the auditory and visual modality and served as a cue for attending to either the auditory or visual modality, respectively. The cue was followed by the simultaneous presentation of a target number (i.e., one, two, or three) in both the auditory and visual modality. For example, if the cue was "HEAR," participants were instructed to respond to the target stimuli (presented aurally) and ignore the number that was simultaneously presented on the screen. In the selective attention congruent target (SCT) conditions, the simultaneously presented visual and auditory stimuli were identical. In the selective attention incongruent non-target (SIN; stimulus conflict) conditions, a target number was presented in the cued modality and a non-target number (six, eight, or nine) was simultaneously presented in the uncued modality. The number "seven" was not chosen as a distractor because it contains a double syllable and was not easily matched to the duration of the other aural stimuli. In the selective attention incongruent target (SIT; stimulus and response conflict) conditions, non-identical target numbers (one, two, or three) were simultaneously presented in the cued and uncued modalities. In the divided attention condition, the cue word was "BOTH" and participants were instructed to respond to the target number that appeared in both the auditory or visual modality (congruent trials) or in a single sensory modality. The results from the divided attention condition will be presented in a separate manuscript.

Each experimental condition was repeated 27 times. The inter-trial interval was either 4, 6, or 8 s and trial order was pseudorandomly presented across nine separate FMRI runs. The duration of the inter-trial interval was varied to prevent the development of temporal expectations, and to allow for the best sampling of the hemodynamic response in the regression model [Burock et al., 1998]. All participants briefly practiced the task in a separate session prior to scanning, which was discontinued when task competency was demonstrated (e.g., responding to auditory targets on auditory trials).

In addition to the active experimental tasks presented above, all participants were also asked to engage in periods of extended passive mental activity so that functional connectivity could be determined. Specifically, following three runs of the complex attention task described above, subjects were asked to relax and passively stare at a fixation cross (visual angle = 1.54°) for three minutes. The sequence of complex attentional and extended rest runs were repeated three times, resulting in three resting runs collected for a total of 9 min.

MR Imaging

At the beginning of the scanning session, a single, high resolution T1 [TE (echo time) = 4.76 ms, TR (repetition time) = 12 ms, 20° flip angle, number of excitations (NEX) = 1, slice thickness = 1.5 mm, FOV (field of view) = 256 mm, resolution = 256 × 256] anatomic image was collected on a 1.5 Tesla Siemens Sonata scanner. During each of the nine functional runs, 164 echo-planar images were acquired using a single-shot, gradient-echo echoplanar pulse sequence [TR = 2,000 ms; TE = 36 ms; flip angle = 90°; FOV = 256 mm; matrix size = 64 × 64]. Twenty-eight contiguous, sagittal 5.5-mm thick slices were selected to provide whole-brain coverage (voxel size: 4 × 4 × 5.5 mm^3). The first image of each run was eliminated to account for T1 equilibrium effects, leaving a total of 1,467 images for the final analyses.

Image Processing and Statistical Analyses

Functional images were generated using Analysis of Functional NeuroImages (AFNI) software package [Cox, 1996]. Time series images were spatially registered in both two- and three-dimensional space to minimize effects of head motion, temporally interpolated to correct for slice-time acquisition differences and de-spiked. A voxelwise finite impulse response deconvolution was then used to derive the hemodynamic response function for each condition relative to the baseline state (fixation plus ambient noise) based on the first nine images (18 s) post-stimulus onset.

The general form of a single condition deconvolution analysis (http://afni.nimh.nih.gov/afni/doc/manual/3dDeconvolve) based on nine parameters can be represented by the following equation:

$$\begin{aligned} Y(n) &= \beta_0 + \beta_1 n + h(0)f(n) + h(1)f(n-1) \\ &\quad + \ldots + h(8)f(n-8) + e(n) \\ &= \beta_0 + \beta_1 n + \sum_{i=0}^{8} h(i)f(n-i) + e(n), \quad (1) \end{aligned}$$

where the observed signal (Y) at each time-point (n) is defined as a linear combination of a constant term (β_0), linear (β_1) or higher-order polynomial term, and the presence of the experimental condition (denoted by the vector h) multiplied by a binary vector (f) indicating whether the experimental condition occurred on the current and/or previous eight images.

The solution is optimized by minimizing the sum of squares of the residual error term, represented by $e(n)$.

Three different deconvolution models were constructed in the current experiment to parse the variance associated with error trials at the subject level and control for differences in the number of trials. In the first deconvolution model [hereafter referred to as the untailored model; see Eq. (2)], each condition (S), occurring from 1 to j, was modeled with a single regressor in the design matrix regardless of task accuracy

$$Y(n) = \beta_0 + \beta_1 n + \sum_{s=1}^{j} \sum_{i=0}^{8} h_{(C+I)_S}(i) f_{(C+I)_S}(n-i) + e(n), \quad (2)$$

Where $(C+I)_S$ represents both the correct (C) and incorrect (I) trials for each condition S. The total number of trials (defined by the binary vector $f_{(C+I)_S}$) that was used to estimate the HRF for each S was not parsed by incorrect and correct trials (i.e., variance associated with error included in HRF) and was therefore equal to 27 occurrences per condition.

In the second deconvolution model [hereafter referred to as the tailored model; see Eq. (3)], each condition S was modeled with either one or two regressors dependent on whether the subject made an incorrect response for that particular condition. In this model, the variance associated with correct and incorrect trials was parsed, and the number of trials used to model the correct HRF was dependent on individual subject's performance.

$$Y(n) = \beta_0 + \beta_1 n + \sum_{s=1}^{j} \sum_{i=0}^{8} h_{C_S}(i) f_{C_S}(n-i) + \sum_{s=1}^{j} \sum_{i=0}^{8} h_{I_S}(i) f_{I_S}(n-i) + e(n). \quad (3)$$

Note that the trials for each condition S are separated based on correct (f_{C_S}) and incorrect (f_{I_S}) occurrences. Therefore, tailored and untailored models differed both in terms of variance parsing based on errors (included or isolated) and in terms of the number of trials used to estimate the HRF. For example, the HRF from the untailored model for the SIT trials contained variance from both correct and error trials (always 27 occurrences) whereas the SIT HRF from the tailored model were based strictly on correct trials (27 - Σf_{I_S}). Although error trials were explicitly modeled with a separate regressor, the majority of participants had insufficient errors to derive a reliable HRF for the error trials in any of the conditions (see behavioral results and Supporting Information Table I).

The third model [hereafter referred to as the equated model; see Eq. (4)] accounted for the difference in trial occurrences by equating the number of trials used to model the HRF based on the number of errors made by each subject. Specifically, given × number of errors, × number of randomly selected correct trials were coded into a separate regressor (RC). The equated model therefore did not parse the variance associated with error trials, but was equivalent to the tailored model [Eq. (3)] in terms of the number of trials used to estimate the HRF.

$$Y(n) = \beta_0 + \beta_1 n + \sum_{s=1}^{j} \sum_{i=0}^{8} h_{(C^*+I)_S}(i) f_{(C^*+I)_S}(n-i) + \sum_{s=1}^{j} \sum_{i=0}^{8} h_{RC_S}(i) f_{RC_S}(n-i) + e(n), \quad (4)$$

where $f_{(C^*+I)_S}$ consists of a subset of f_{C_S} and all the trials of f_{I_S} from Eq. (3). Specifically, a randomly selected subset of f_{C_S} is defined as f_{RC_S} and the remaining trials as $f_{(C^*)_S}$, in which $f_{C_S} = f_{(C^*)_S} + f_{RC_S}$ holds true. The random correct trials regressor f_{RC_S} had the same number of trials as the incorrect trials regressor [f_{I_S}; Eq. (3)] for each subject for each condition and therefore controlled for the number of trials used to generate the HRF.

An estimation of percent signal change was then calculated for each condition by averaging the beta coefficients for the images occurring six to ten seconds post-cue onset (peak of the hemodynamic response function) and dividing by the average model intercept (β_0) across all experimental runs. The percent signal change maps were then converted to a 1 mm^3 standard stereotaxic coordinate space [Talairach and Tournoux, 1988] and spatially blurred using a 6-mm Gaussian filter.

Repeated-measures ANOVAs were then conducted to determine how functional activation varied as a factor of the different deconvolution models across the three (SCT, SIT, SIN) different selective attention trial types. Specifically, the tailored model [Eq. (3)] was first contrasted against the untailored model [Eq. (2)] to determine the effect of error modeling on patterns of functional activation. The second series of ANOVAs tested the tailored model against the equated model [Eq. (4)] to confirm that findings were not related to differences in the number of trials included in the modeling of the HRF.

Functional connectivity analyses were conducted using standard methodology [Fox et al., 2005] based on data from the extended resting task (maintaining visual fixation for 9 min). Briefly, individual anatomical images (i.e., T1) were first segmented into maps of white matter, gray matter and cerebral spinal fluid (CSF); the resultant CSF and white matter masks were then used to obtain an average time-series for these tissues during the extended resting state run. Next, all six movement parameters, the region of interest (ROI)-based time-series for CSF and white matter, a constant term, and a linear term were entered into a linear regression against the extended resting state time-series. A global grey matter term was not entered into the regression to minimize likelihood of increased anti-correlations [Fox et al., 2009; Murphy et al., 2009]. The residual time-series data were then transformed into a standardized

TABLE I. Clusters exhibiting main effect of condition in untailored model

		Activation in main effect						Follow-up comparisons		
Region	Side	BA	*X*	*Y*	*Z*	Volume (ml)	Average *F*-score	SIT > SCT	SIT > SIN	SIN > SCT
Frontal lobe										
Rostral ACC	B	24/32	2	33	18	3.007	7.735	X	X	
Dorsal ACC/Pre-SMA/SMA	B	6/24/32/33	0	12	42	10.998	7.416	X	X	
Premotor cortex	R	6	16	−6	57	1.488	7.522	X	X	
	L	6/9	−35	−2	45	6.571	7.909	X	X	
Ventrolateral prefrontal	R	13/44/45/47	36	19	4	2.486	7.384		X	
cortex and insula	L		−37	17	3	8.113	8.628	X	X	
Temporal lobe										
Middle/superior temporal and supramarginal gyri	L	13/22/37/40	−50	−43	12	5.674	7.097	X	X	
Superior temporal and post-central gyri	L	41/42/43	−55	−19	19	1.437	7.367	X		
Parietal lobe										
Posterior parietal cortex	L	3/4/40/7	−28	−45	46	7.343	7.285	X	X	
Precuneus, cuneus and posterior cingulate gyrus	B	7/30/31	−11	−65	36	6.546	7.527	X		X
Precuneus	L	7	−26	−66	26	3.337	8.763	X		
Occipital lobe										
Lingual gyrus and cuneus	R	17/18/23	9	−76	8	1.793	7.314	X		
Subcortical										
Thalamus, sub-thalamic nuclei and caudate	B		4	−11	−2	5.502	8.328	X	X	
Cerebellum										
Vermis, Lobule VI and Crus I	R		8	−65	−16	1.935	7.451	X		

Note: Side refers to the hemisphere showing activation where B = bilateral; L = left, and R = right hemisphere. The Brodmann area (BA), the center of mass in Talairach coordinates (*X*, *Y*, *Z*) and volume in milliliters (ml) are specified for each area of activation in the main effect of condition. Significant follow-up paired t-test comparisons are marked with an *X*.

coordinate space [Talairach and Tournoux, 1988]. Paired *t* tests were then conducted to determine the brain areas that demonstrated either a stronger correlation (both correlations positive), a stronger anti-correlation (both correlations negative), or opposing correlations (positively correlated with one seed and negatively correlated with another seed) using empirically derived ROIs from the dMFC.

To minimize false positives, a parametric threshold corresponding to $P < 0.005$ and a minimum cluster size of 1.408 ml (i.e., 16 original voxels) was adopted for all whole brain functional analyses [Forman et al., 1995]. These thresholds were determined based on 10,000 Monte Carlo simulations demonstrating that the chance probability of obtaining a significant activation cluster for an entire volume for all analyses (Type I error) was less than $P = 0.05$.

RESULTS

Behavioral Data

Two repeated-measures ANOVAs were performed to examine condition-specific (SCT, SIN, SIT) differences in accuracy and reaction time during the selective attention conditions (see Fig. 1B,C). For all behavioral and functional analyses, data was collapsed across modality for focused attention (auditory or visual), resulting in a total of 54 trials per condition. The first ANOVA indicated a significant main effect of condition, ($F_{2,46} = 35.88$, $P < 0.001$), with significantly more errors being committed on incongruent target trials (2.25 SIT errors = 95.8% accuracy) compared to both congruent (0.19 SCT errors = 99.6% accuracy; $t_{23} = -6.38$, $P < 0.001$) and incongruent non-target trials (0.42 SIN errors = 99.2% accuracy; $t_{23} = -6.20$, $P < 0.001$; see Fig. 1B). There were no significant differences between congruent and incongruent non-target trials ($P > 0.10$). It is notable that the total number of errors made in all three conditions was extremely low, suggesting that performance on the task was near ceiling (see Supporting Information Table I).

A second ANOVA was conducted on individual subject's median reaction time for correct trials only. A significant main effect of condition was observed, $F_{2,46} = 22.82$, $P < 0.001$, and follow-up tests indicated that response times were faster for congruent (399.2 ms) compared to both incongruent non-target (477.9 ms; $t_{23} = -5.68$, $P < 0.001$) and incongruent target trials (543.0 ms; $t_{23} = -5.10$,

$P < 0.001$; see Fig. 1C). In addition, incongruent non-target trials were also significantly faster than incongruent target trials ($t_{23} = -3.35$, $P < 0.005$). These behavioral results demonstrate the expected monotonic increase in interference as a function of distractor type, suggesting that the experimentally manipulated level of conflict was successful.

Functional Data

Tailored vs. untailored model

A 2 × 3 (Model × Condition) repeated measures ANOVA was first conducted to examine the effects of parsing out the variance associated with relatively few errors in the selective attention conditions (tailored model) compared to the effects of not modeling error responses (untailored model). There were several regions that exhibited a significant main effect of model or condition that were not also involved in the Model × Condition interaction. Specifically, a main effect of model (untailored > tailored) was observed in the right supramarginal gyrus and inferior parietal lobule (BA 40; 1.455 ml; center of mass $X = 44$, $Y = -44$, $Z = 40$). A main effect of condition was observed in the left middle/superior temporal gyri extending into the inferior parietal lobe (BAs 13/21/22/40; 2.482 ml; center of mass $X = -51$, $Y = -42$, $Z = 12$), with greater activation in SIT relative to SCT across both models. A main effect of condition was also observed in the left posterior parietal cortex extending into the cuneus (BAs 2/3/7/40; 10.079 ml; center of mass $X = -24$, $Y = -56$, $Z = 39$), with greater activity being observed for SIT relative to both SCT and SIN.

In addition, widespread cortical, subcortical and cerebellar activation was observed for the Model × Condition interaction effect (see Fig. 2A). These regions included a large cluster within the bilateral dMFC, including the rostral and dorsal aspects of the anterior cingulate gyrus (BAs 24/32) extending into the pre-supplementary motor area/supplementary motor area (pre-SMA/SMA; BAs 6/8), as well as the bilateral DLPFC (BAs 9/45/46). Additional clusters of interest included the bilateral ventrolateral prefrontal cortex (VLPFC) and anterior insula (BAs 44/45/47/13), bilateral middle/superior frontal gyrus (BA 6), right heteromodal cortical area of the posterior superior temporal gyrus (BAs 22/39), the left inferior parietal lobule (BA 40), right temporo-parietal juncture (BA 39), bilateral thalamus, hippocampus and caudate nucleus. To further quantify this extensive interaction effect, we conducted separate one-way ANOVAs to identify regions exhibiting a main effect of condition for both the untailored and tailored models. Identified clusters of activation were then subjected to pairwise t tests to determine which of the three contrasts (SCT vs. SIN; SCT vs. SIT; SIN vs. SIT) were contributing to the observed variance.

In the untailored analyses (Fig. 2B; Table I), the main effect of condition resulted in extensive activation of the bilateral dMFC, including the rostral and dorsal regions of

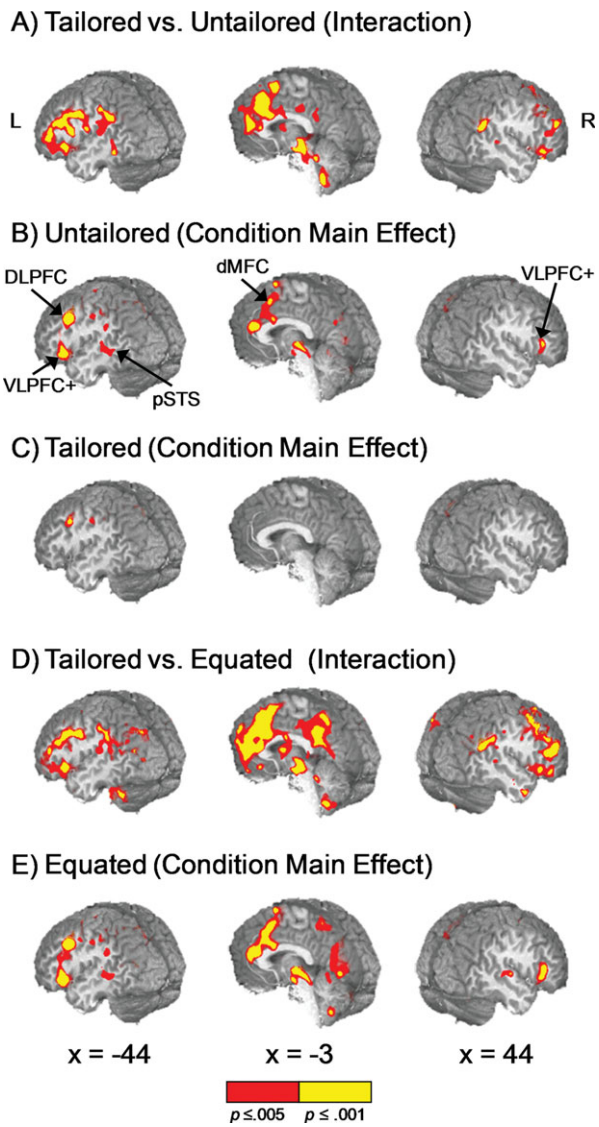

Figure 2.

Panel **A** displays regions that exhibited a significant model × condition interaction effect when the tailored and untailored models were compared. Regions exhibiting a main effect of condition are presented for the untailored (Panel **B**) and tailored (Panel **C**) models. Significant areas of activation in the untailored model included (a) bilateral ventrolateral prefrontal cortex and anterior insula (VLPFC+), (b) left posterior superior temporal sulcus (pSTS), (c) left dorsolateral prefrontal cortex, and (d) bilateral dorsal medial frontal cortex (dMFC). Note the absence of a main effect of condition within the dMFC and several other structures in the tailored model. Panel **D** displays regions that exhibited a significant model × condition interaction effect when the tailored and equated models were compared, with Panel E exhibiting the main effect of condition for the equated model. Locations of slices are given according to the Talairach atlas. Color scale represents significance levels (red: $0.001 < P \leq 0.005$, yellow: $P \leq 0.001$).

TABLE II. Clusters exhibiting main effect of condition in tailored model

		Activation in main effect						Follow-up comparisons		
Region	Side	BA	*X*	*Y*	*Z*	Volume (ml)	Average *F*-score	SIT > SCT	SIT > SIN	SIN > SCT
Frontal lobe										
Premotor cortex	L	6/9	−35	−2	47	1.470	7.008	X		
Parietal lobe										
Posterior parietal lobule	L	7/40	−31	−40	44	2.479	6.985		X	
Precuneus	L	7	−19	−65	34	3.195	7.573	X		

Note: Side refers to the hemisphere showing activation where L = left. The Brodmann area (BA), the center of mass in Talairach coordinates (*X*, *Y*, *Z*) and volume in milliliters (ml) are specified for each area of activation in the main effect of condition. Significant follow-up paired *t* test comparisons are marked with an *X*.

the anterior cingulate gyrus (BAs 24/32/33), pre-SMA and small portion of SMA (BA 6). Follow-up *t* tests (see Table I) indicated that activation within the dMFC was greater for incongruent target compared to both congruent and non-target trials (SIT > SCT and SIT > SIN), with no evidence of increased activation for SIN compared to SCT trials. Additional regions demonstrating increased activity for the SIT relative to SCT and SIN trials included the left VLPFC, anterior aspects of the insula, bilateral pre-motor cortex, left posterior middle/superior temporal gyrus, left posterior parietal cortex, bilateral thalamic and subthalamic nuclei. In addition, increased activation during incongruent compared to congruent trials (SIT > SCT) was also observed in the left auditory cortex, bilateral precuneus and cuneus, right lingual gyrus and cuneus, and right cerebellum. Greater activation for incongruent target compared to non-target trials (SIT > SIN) was observed within the right VLPFC and anterior insula. Finally, greater activation for the SIN compared to SCT trials was also observed within the precuneus.

Significant regions demonstrating a main effect of condition for the tailored model (Fig. 2C; Table II) included the left premotor area and the left precuneus (SIT > SCT), as well as the left superior and inferior parietal lobules (SIT > SIN). Although a main effect of condition was not present in the dMFC in the tailored model, pairwise comparisons on the individual trials were conducted to examine a priori hypotheses of increased activation for the SIT trials within the dMFC utilizing a more liberal threshold ($P < 0.005$; 0.528 ml). Results indicated that there was no evidence of increased activation for SIN compared to SCT trials within the dMFC, even at the lower threshold. However, three focal clusters of increased activation for SIT compared to SCT activation were observed within the bilateral ACC (BA 24; 0.553 ml; center of mass $X = 3$, $Y = 14$, $Z = 26$), the right dACC extending into the pre-SMA (BAs 24/6; 0.673 ml; center of mass $X = 6$, $Y = 6$, $Z = 47$), and the bilateral pre-SMA and SMA (BA 6; 0.749 ml; center of mass $X = -2$, $Y = 2$, $Z = 63$).

The results from the SIT versus SCT comparison across both tailored ($P < 0.005$; 0.528 ml) and untailored ($P < 0.005$; 1.408 ml) analyses are displayed together in Figure 3 in binary format for comparison purposes. In addition to the reduced volume of activation within these dMFC clusters for the tailored model, a unique cluster of rostral ACC (superior and anterior to genu of corpus callosum) activity was also present in the untailored model when the statistical variance associated with error trials was not parsed, suggesting a more specific role for this structure in monitoring errors.

Tailored vs. equated model

In addition to the parsing of error variance, the tailored and untailored models also differed in terms of number of trials used to calculate the HRF. To ensure that the above results were not due to this trial differential, an additional deconvolution analysis was conducted in which correct and incorrect trials were not parsed but the overall number of trials was equated to the tailored analyses on a per-subject basis [see equated model; Eq. (4)]. An identical 2 × 3 (Model × Condition) ANOVA was then conducted to compare the tailored and equated models. As demonstrated in Figure 2D, the results for the model by condition interaction for the tailored/equated ANOVA were similar to the tailored/untailored ANOVA in all key regions (dMFC, DLPFC, parietal lobes, VLPFC and anterior insula). In addition, the main effect of condition (and subsequent follow-up tests) was similar in both the equated and untailored models (see Fig. 2E) for all key areas, suggesting that previous differences in the tailored and untailored models were not an artifact due to the different number of trials. Finally, the volume and magnitude of activation for the statistical maps (i.e., main effect of condition) was greater in the equated compared to untailored model (see Fig. 2B,E), which is likely a result of the greater proportion of errors to correct trials in the equated model.

Functional Connectivity Analyses

To further evaluate the putative role of the dMFC in cognitive control, four voxel-wise seed-based correlation

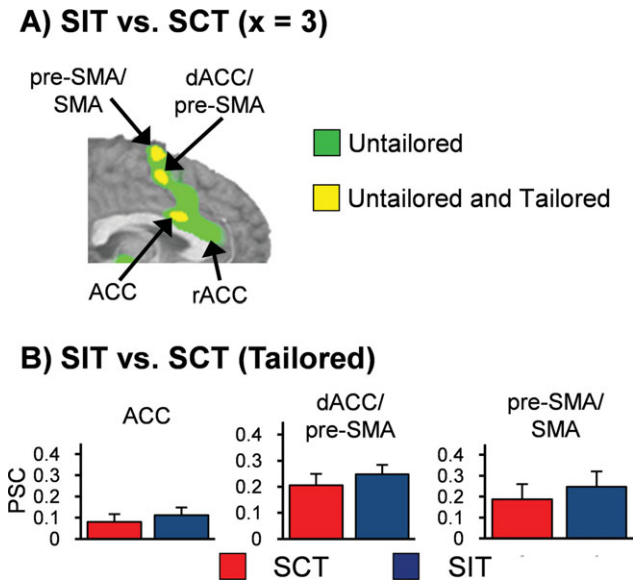

Figure 3.

Panel **A** is a binary bichromatic map depicting regions that exhibited statistically greater activation for SIT compared to SCT trials in the untailored model (green coloring) or both the untailored and tailored model (yellow coloring). Panel **B** presents mean percent signal change (PSC) values for the SCT (red bar), and SIT (blue bar) conditions for the three dMFC clusters from the tailored model (error bars = 2 × standard error of the mean). Location of slice (×) is given according to the Talairach atlas.

analyses were conducted to directly compare resting-state connectivity between the dMFC and other brain regions [Fox et al., 2005].[1] Three of the seed regions for the connectivity analyses were based on clusters derived from dMFC regions of interest (ROI) from the SIT versus SCT comparison (see Fig. 3) in the tailored model (ACC center of mass: $X = 3$, $Y = 14$, $Z = 26$; dACC/pre-SMA center of mass: $X = 6$, $Y = 6$, $Z = 47$; pre-SMA/SMA center of mass: $X = -2$, $Y = 2$, $Z = 63$). The last seed was derived from the unique activity observed in the rACC during the untailored analysis (rACC: $X = 1$, $Y = 31$, $Z = 17$). Pair-wise t tests were then performed to examine the magnitude of resting state correlations amongst the different seed pairs.

Results indicated that connectivity between the dMFC and other brain regions was heavily mediated by the rostral-inferior to posterior-dorsal organization of the seeds (see Fig. 4). Specifically, the rACC demonstrated a positive correlation with the DMN, including clusters within the superior frontal gyri (BAs 8/9), the posterior cingulate cortex (BAs 23/29/30/31), temporal-parietal areas (BAs 39/40), bilateral inferior to middle temporal gyri (BAs 20/21/38), parahippocampal gyri (BAs 28/35), and left inferior frontal gyrus (BA 47). In addition, the rACC also demonstrated a negative relationship within the bilateral DLPFC (BAs 9/10/46), bilateral VLPFC and insula (BAs 44/45/47/13), premotor and sensorimotor cortices (BAs 2/3/4/6), bilateral posterior parietal cortex (BAs 2/40), and bilateral precuneus (BA 7), a network which has previously been associated with several different cognitive tasks [Cabeza and Nyberg, 2000]. The magnitude of connectivity relationships between the dMFC and the two networks decreased in magnitude and typically reversed in sign within the ACC seed, and then became maximally inverted in magnitude and polarity within the dACC/pre-SMA seed (i.e., maximal anti-correlation with DMN and maximal correlation with task-related network). The magnitude of the connectivity relationships between primary nodes from the DMN and task-related networks declined within the pre-SMA/SMA proper from the dACC/pre-SMA levels.

DISCUSSION

The current experiment provided a novel examination of the role of the dMFC in various forms of conflict and error monitoring during a multimodal numeric Stroop task with relatively few error trials. Functional results demonstrated a role for the dMFC in error-processing and conclusively highlighted the importance of parsing the variance associated with error and high conflict trials in cognitive control studies even when minimal errors are present. Behavioral data indicated that task performance was detrimentally affected by the presence of conflicting stimuli in an unattended sensory modality, corroborating the notion that limited attentional resources exist for processing conflicting, task relevant and temporally congruent multimodal stimuli [Johnson and Zatorre, 2005; Mayer et al., 2009]. Response times monotonically increased dependent on whether the incongruent multimodal distractors were based on stimulus (SIN) or stimulus and response selection (SIT) conflict. However, functional results indicated that the dMFC may only be activated in response to conditions that involve motor conflict (SIT trials) when error variance is properly modeled.

A novel statistical approach was used to either isolate or include variance associated with error trials across the three different conflict conditions (SCT = no conflict; SIN = stimulus conflict; SIT = stimulus and motor conflict). Conflict-driven activity (i.e., main effect of condition) within the dMFC was present only when the variance associated with errors was not statistically parsed (i.e., untailored model). Unlike previous experiments where error rates were purposely increased by degrading stimulus properties [Brown and Braver, 2005; Garavan et al., 2002, 2003; Lutcke and Frahm, 2008], results from the untailored model provide new insight on the effects of a relatively few error trials. Current findings suggest that incorrect trials disproportionally contribute to hemodynamic activation within the dMFC, which is likely a result

[1]An identical series of analyses using 12 mm spheres located at the centers of mass of each of the seed clusters was performed to control for differences in seed region volume and yielded similar results.

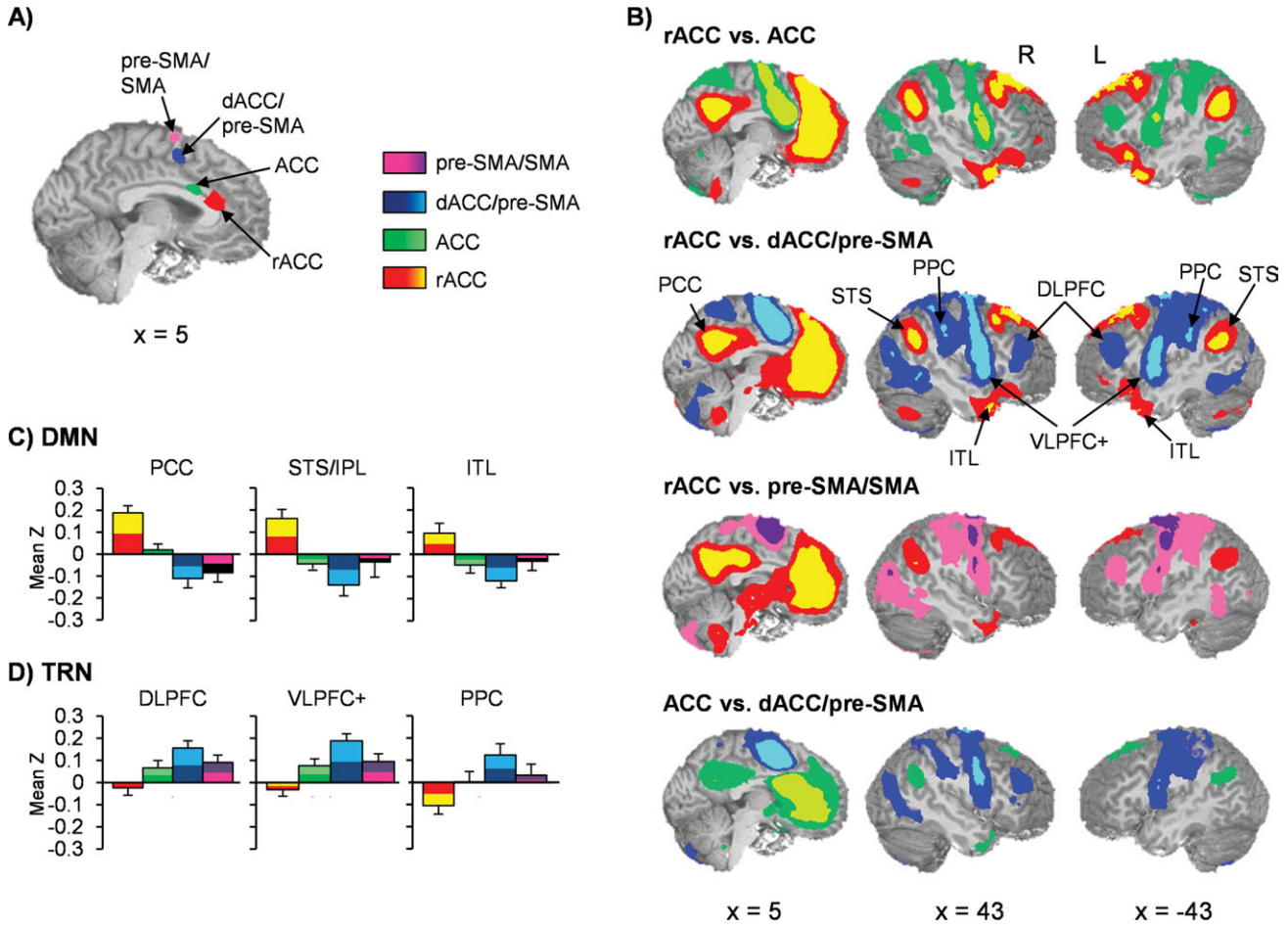

Figure 4.

Panel **A** displays the location of the four clusters from the SIT versus SCT comparisons that were used as seeds in functional connectivity analyses. Panel **B** exhibits selected pairwise contrasts between the rostral anterior cingulate cortex (rACC; yellow/red), anterior cingulate cortex (ACC; green colors), dorsal anterior cingulate extending into the pre-supplementary motor area (dACC/pre-SMA; blue colors), and pre-SMA/supplementary motor area proper (pre-SMA/SMA; pink/purple colors). Clusters that survived false-positive correction across pairwise comparisons were bichromatically color-coded to be consistent with seed color scheme (i.e., increased connectivity for dACC/pre-SMA represented with blue shades for all pair-wise comparisons whereas increased connectivity with rACC color-coded with yellow and red). Panel C demonstrates connectivity (mean Z score) between regions (PCC = posterior cingulate cortex; STS/IPL = superior temporal sulcus/inferior parietal lobule; ITL = inferior temporal lobule) of the default-mode network (DMN) with the different seeds (error bars = 2 × standard error of the mean). Panel **D** shows a similar display for regions (DLPFC = dorsolateral prefrontal cortex; VLPFC+ = ventrolateral prefrontal cortex and anterior insula; PPC = posterior parietal cortex) of the task-related network (TRN). Regions from both networks were defined based on the comparison of the rACC versus dACC/pre-SMA (Panel B, second row). Locations of slices are given according to the Talairach atlas.

of the strong affective response that occurs following infrequent errors [Luu et al., 2003; Taylor et al., 2006]. Additional analyses (equated versus tailored model) confirmed that the disproportionate activity observed in dMFC and lateral prefrontal cortex was not a result of a decreased number of trials in the tailored model. Thus, current findings underscore the critical importance of controlling for error-related variance in conflict experiments regardless of the number of errors committed. However, current findings also require replication in an independent sample and/or additional simulations to confirm whether the widespread cortical activation associated with a few error trials is dependent on task context (e.g., cognitive control experiments) or occurs across a variety of cognitive paradigms.

Although the segregation of conflict and error variance seems straight-forward, it is notable that only a minority

(5/34) of studies reviewed in a recent meta-analysis [Roberts and Hall, 2008] of pure conflict tasks (e.g., Stroop, Simon, and flanker tasks) categorized error and high conflict trial variance separately during functional analyses. The frequency of errors tends to be low when these pure conflict tasks are performed by healthy controls. However, the error rate is typically greater for high conflict trials, thereby introducing a potential confound into the experimental design. Therefore, although the results from this meta-analysis and individual studies were interpreted to be clearly suggestive of the dMFC role in conflict-related mediation [Roberts and Hall, 2008], current and previous [Garavan et al., 2003; Taylor et al., 2006] results suggest the need for accurately modeling error variance even in the context of relatively sparse error trials.

Consistent with previous findings [Liston et al., 2006; van Veen et al., 2001], a direct comparison of pure stimulus conflict trials (SIN) and congruent trials did not result in increased dMFC or lateral prefrontal activation for either the tailored or untailored model. In contrast, trials that involved both stimulus and response selection conflict (SIT) resulted in activation within three smaller dMFC clusters, as well as activation of several frontal and parietal regions previously associated with top-down attentional control. The first dMFC cluster was located within the anterior cingulate gyrus proper (BA 24), superior to the genu of the corpus callosum (Cluster 7, [Beckmann et al., 2009]; i3-i4, [Margulies et al., 2007]). The second dMFC cluster was located on the boundary between the dorsal ACC and pre-SMA (BAs 24/32/6; Clusters 4 and 5, [Beckmann et al., 2009]; s2-s3, [Margulies et al., 2007]), primarily corresponding to area RCZp [Picard and Strick, 1996], and involving the regions of the dMFC most typically associated with error-processing and conflict monitoring in prior studies [Beckmann et al., 2009]. Finally, the third dMFC cluster was located within the pre-motor cortex on the border of the pre-SMA and SMA proper (BA 6).

SIT trials differed from SIN trials both in terms of level of conflict (i.e., greater conflict in SIT due to more salient target distractors) as well as the additional requirements of response selection and the inhibition of competing motor responses, both of which may have contributed to the increase in dMFC activity during SIT compared to SCT trials. Thus, previous [Liston et al., 2006; van Veen et al., 2001] and current results indicate that the mere presence of stimulus conflict does not appear to be sufficient to drive activity within dMFC and lateral prefrontal cortices. Rather, the requirements of response selection and/or response inhibition appear to be critical for producing dMFC activity during conflict trials, which may be a result of the rich interconnectivity that exists between this region and the motor system [Picard and Strick, 1996]. There are several independent lines of research that question a ubiquitous role for the dMFC in processing all forms of conflict. Single cell primate recording studies fail to observe conflict-related activity in the ACC [Ito et al., 2003; Nakamura et al., 2005]. Human lesion studies have not observed any deficits in cognitive control for patients with cingulate damage [Fellows and Farah, 2005] or have attributed conflict detection to lateral rather than medial prefrontal cortex [Swick and Turken, 2002].

The dMFC has been shown to have considerable heterogeneity in terms of both functional [Margulies et al., 2007] and anatomical [Beckmann et al., 2009] connectivity. Current results indicated that sub-regions of the dMFC showed strong connectivity with two large-scale networks previously associated with either externally-driven, attention demanding tasks or internal states such as daydreaming [Fox et al., 2005]. However, the magnitude and sign of these connectivity relationships was critically mediated by a caudal-superior to a rostral-inferior gradient. Specifically, the dACC/pre-SMA (BAs 24/6) demonstrated the highest functional connectivity coefficients within the lateral prefrontal, posterior parietal and pre-motor cortex. Collectively these regions form a network that has been implicated in the top-down allocation of attentional resources [Cabeza and Nyberg, 2000; Fox et al., 2005], and supports the suggestion that the dACC/pre-SMA plays an integral role in attentional control [Botvinick et al., 2001; Carter and van Veen, 2007; Carter et al., 1998].

The dACC/pre-SMA also demonstrated the strongest anti-correlation with the DMN [Buckner et al., 2008; Raichle et al., 2001], where changes in the pattern of activation have been shown to precede overt behavioral errors [Eichele et al., 2008]. In contrast, the rACC demonstrated the highest correlations with the DMN and the highest anti-correlations with the task-related attentional network described above. The rACC was the one region of the dMFC that demonstrated unique activation during a comparison of high (SIT) and low (SCT) conflict conditions from the untailored model (see Fig. 3), suggesting a larger role in error processing. Localization of error processes to the rACC is consistent with previous imaging studies [Garavan et al., 2003; Ullsperger and von Cramon, 2001] as well as data demonstrating that electrophysiological error responses predict FMRI activation in the rACC [Debener et al., 2005].

There are several potential limitations to the current study. First, a cue was utilized to direct attention to a specific sensory modality, which may have reduced dMFC activity during the various conflict conditions [Aarts et al., 2008]. Second, the current experiment attempted to isolate pure stimulus conflict (SIN condition) versus stimulus and response conflict (SIT condition). However, the degree of stimulus conflict was also greater in the SIT compared to SIN condition, such that the observed dMFC activity could have been the result of a conflict threshold effect rather than due to response selection conflict. Future studies that vary the level of pure stimulus conflict without introducing a motor component could address this question. Likewise, ACC activity has been observed during trials that do not contain conflicting responses [Roelofs et al., 2006], during decisional stages when motor responses are not required [Pochon et al., 2008], during the subjective attribution of value judgment [Holroyd and Coles, 2008], as

well as several other aspects of regulatory functioning that were not evaluated in the current experiment.

In summary, current results conclusively demonstrate that the parsing of conflict and error-related variance is a necessary step for determining the role of the dMFC activity during cognitive control experiments even during protocols when only a minimal number of errors are expected. Although this has been done more frequently in recent studies [Brown and Braver, 2007; Nieuwenhuis et al., 2007], prior results that did not statistically control for errors should be critically evaluated as the reported dMFC activation may be a result of error processing rather than conflict. In addition, pure stimulus conflict trials without a conflicting motor response did not result in significantly different activity within the dMFC or other prefrontal cortical areas compared to no-conflict trials, suggesting that requirements of response selection and inhibition may drive dMFC activity. Results also suggest that variance associated with errors was uniquely localized to the rACC, which also demonstrates increased functional connectivity with the DMN and strong anti-correlations with frontal and parietal structures involved in top-down attentional control.

ACKNOWLEDGMENTS

Special thanks to Diana South and Ranee Flores for assistance with data collection.

REFERENCES

Aarts E, Roelofs A, van TM (2008): Anticipatory activity in anterior cingulate cortex can be independent of conflict and error likelihood. J Neurosci 28:4671–4678.

Banich MT, Milham MP, Atchley RA, Cohen NJ, Webb A, Wszalek T, Kramer AF, Liang Z, Barad V, Gullett D, Shah C, Brown C (2000): Prefrontal regions play a predominant role in imposing an attentional "set": Evidence from fMRI. Brain Res Cogn Brain Res 10:1–9.

Beckmann M, Johansen-Berg H, Rushworth MF (2009): Connectivity-based parcellation of human cingulate cortex and its relation to functional specialization. J Neurosci 29:1175–1190.

Botvinick MM, Nystrom LE, Fissell K, Carter CS, Cohen JD (1999): Conflict monitoring versus selection-for-action in anterior cingulate cortex. Nature 402:179–181.

Botvinick MM, Braver TS, Barch DM, Carter CS, Cohen JD (2001): Conflict monitoring and cognitive control. Psychol Rev 108: 624–652.

Braver TS, Reynolds JR, Donaldson DI (2003): Neural mechanisms of transient and sustained cognitive control during task switching. Neuron 39:713–726.

Brown JW, Braver TS (2005): Learned predictions of error likelihood in the anterior cingulate cortex. Science 307:1118–1121.

Brown JW, Braver TS (2007): Risk prediction and aversion by anterior cingulate cortex. Cogn Affect Behav Neurosci 7:266–277.

Buckner RL, Andrews-Hanna J, Schacter D (2008): The brain's default network: Anatomy, function, and relevance to disease. Ann N Y Acad Sci 1124:1–38.

Burock MA, Buckner RL, Woldorff MG, Rosen BR, Dale AM (1998): Randomized event-related experimental designs allow for extremely rapid presentation rates using functional MRI. NeuroReport 9:3735–3739.

Cabeza R, Nyberg L (2000): Imaging cognition II: An empirical review of 275 PET and fMRI studies. J Cogn Neurosci 12:1–47.

Carter CS, van Veen V (2007): Anterior cingulate cortex and conflict detection: An update of theory and data. Cogn Affect Behav Neurosci 7:367–379.

Carter CS, Braver TS, Barch DM, Botvinick MM, Noll D, Cohen JD (1998): Anterior cingulate cortex, error detection, and the online monitoring of performance. Science 280:747–749.

Carter CS, Macdonald AM, Botvinick M, Ross LL, Stenger VA, Noll D, Cohen JD (2000): Parsing executive processes: Strategic vs. evaluative functions of the anterior cingulate cortex. Proc Natl Acad Sci USA 97:1944–1948.

Cox RW (1996): AFNI: Software for analysis and visualization of functional magnetic resonance neuroimages. Comp Biomed Res 29:162–173.

Davis KD, Taylor KS, Hutchison WD, Dostrovsky JO, McAndrews MP, Richter EO, Lozano AM (2005): Human anterior cingulate cortex neurons encode cognitive and emotional demands. J Neurosci 25:8402–8406.

Debener S, Ullsperger M, Siegel M, Fiehler K, von Cramon DY, Engel AK (2005): Trial-by-trial coupling of concurrent electroencephalogram and functional magnetic resonance imaging identifies the dynamics of performance monitoring. J Neurosci 25:11730–11737.

Dehaene S, Posner MI, Tucker DM (1994): Localization of a neural system for error detection and compensation. Psychol Sci 5: 303–305.

Eichele T, Debener S, Calhoun VD, Specht K, Engel AK, Hugdahl K, von Cramon DY, Ullsperger M (2008): Prediction of human errors by maladaptive changes in event-related brain networks. Proc Natl Acad Sci USA 105:6173–6178.

Falkenstein M, Hohnsbein J, Hoormann J, Blanke L (1991): Effects of crossmodal divided attention on late ERP components. II. Error processing in choice reaction tasks. Electroencephalogr Clin Neurophysiol 78:447–455.

Fellows LK, Farah MJ (2005): Is anterior cingulate cortex necessary for cognitive control? Brain 128:788–796.

Fias W, Reynvoet B, Brysbaert M (2001): Are Arabic numerals processed as pictures in a Stroop interference task? Psychol Res 65:242–249.

Forman SD, Cohen JD, Fitzgerald M, Eddy WF, Mintun MA, Noll DC (1995): Improved assessment of significant activation in functional magnetic resonance imaging (fMRI): Use of a cluster-size threshold. Magn Reson Med 33:636–647.

Fox MD, Snyder AZ, Vincent JL, Corbetta M, Van E, Raichle ME (2005): The human brain is intrinsically organized into dynamic, anticorrelated functional networks. Proc Natl Acad Sci USA 102:9673–9678.

Fox MD, Zhang D, Snyder AZ, Raichle ME (2009): The global signal and observed anticorrelated resting state brain networks. J Neurophysiol 101:3270–3283.

Garavan H, Ross TJ, Murphy K, Roche RA, Stein EA (2002): Dissociable executive functions in the dynamic control of behavior: Inhibition, error detection, and correction. Neuroimage 17: 1820–1829.

Garavan H, Ross TJ, Kaufman J, Stein EA (2003): A midline dissociation between error-processing and response-conflict monitoring. Neuroimage 20:1132–1139.

Gehring WJ, Fencsik DE (2001): Functions of the medial frontal cortex in the processing of conflict and errors. J Neurosci 21: 9430–9437.

Hester R, Fassbender C, Garavan H (2004): Individual differences in error processing: A review and reanalysis of three event-related fMRI studies using the GO/NOGO task. Cereb Cortex 14:986–994.

Holroyd CB, Coles MG (2008): Dorsal anterior cingulate cortex integrates reinforcement history to guide voluntary behavior. Cortex 44:548–559.

Ito S, Stuphorn V, Brown JW, Schall JD (2003): Performance monitoring by the anterior cingulate cortex during saccade countermanding. Science 302:120–122.

Johnson JA, Zatorre RJ (2005): Attention to simultaneous unrelated auditory and visual events: Behavioral and neural correlates. Cereb Cortex 15:1609–1620.

Kerns JG, Cohen JD, MacDonald AW III, Cho RY, Stenger VA, Carter CS (2004): Anterior cingulate conflict monitoring and adjustments in control. Science 303:1023–1026.

Kiehl KA, Liddle PF, Hopfinger JB (2000): Error processing and the rostral anterior cingulate: An event-related fMRI study. Psychophysiology 37:216–223.

Liston C, Matalon S, Hare TA, Davidson MC, Casey BJ (2006): Anterior cingulate and posterior parietal cortices are sensitive to dissociable forms of conflict in a task-switching paradigm. Neuron 50:643–653.

Lutcke H, Frahm J (2008): Lateralized anterior cingulate function during error processing and conflict monitoring as revealed by high-resolution fMRI. Cereb Cortex 18:508–515.

Luu P, Flaisch T, Tucker DM (2000): Medial frontal cortex in action monitoring. J Neurosci 20:464–469.

Luu P, Tucker DM, Derryberry D, Reed M, Poulsen C (2003): Electrophysiological responses to errors and feedback in the process of action regulation. Psychol Sci 14:47–53.

Macaluso E, Driver J (2005): Multisensory spatial interactions: A window onto functional integration in the human brain. Trends Neurosci 28:264–271.

Margulies DS, Kelly AM, Uddin LQ, Biswal BB, Castellanos FX, Milham MP (2007): Mapping the functional connectivity of anterior cingulate cortex. Neuroimage 37:579–588.

Mayer AR, Franco AR, Canive J, Harrington DL (2009): The effects of stimulus modality and frequency of stimulus presentation on cross-modal distraction. Cereb Cortex 19:993–1007.

Menon V, Adleman NE, White CD, Glover GH, Reiss AL (2001): Error-related brain activation during a Go/NoGo response inhibition task. Hum Brain Mapp 12:131–143.

Murphy K, Garavan H (2004): Artifactual fMRI group and condition differences driven by performance confounds. Neuroimage 21:219–228.

Murphy K, Birn RM, Handwerker DA, Jones TB, Bandettini PA (2009): The impact of global signal regression on resting state correlations: Are anti-correlated networks introduced? Neuroimage 44:893–905.

Nakamura K, Roesch MR, Olson CR (2005): Neuronal activity in macaque SEF and ACC during performance of tasks involving conflict. J Neurophysiol 93:884–908.

Nieuwenhuis S, Schweizer TS, Mars RB, Botvinick MM, Hajcak G (2007): Error-likelihood prediction in the medial frontal cortex: A critical evaluation. Cereb Cortex 17:1570–1581.

Picard N, Strick PL (1996): Motor areas of the medial wall: A review of their location and functional activation. Cereb Cortex 6:342–353.

Pochon JB, Riis J, Sanfey AG, Nystrom LE, Cohen JD (2008): Functional imaging of decision conflict. J Neurosci 28:3468–3473.

Raichle ME, MacLeod AM, Snyder AZ, Powers WJ, Gusnard DA, Shulman GL (2001): A default mode of brain function. Proc Natl Acad Sci USA 98:676–682.

Ridderinkhof KR, Ullsperger M, Crone EA, Nieuwenhuis S (2004): The role of the medial frontal cortex in cognitive control. Science 306:443–447.

Roberts KL, Hall DA (2008): Examining a supramodal network for conflict processing: A systematic review and novel functional magnetic resonance imaging data for related visual and auditory stroop tasks. J Cogn Neurosci 20:1063–1078.

Roelofs A, van TM, Coles MG (2006): Anterior cingulate cortex activity can be independent of response conflict in Stroop-like tasks. Proc Natl Acad Sci USA 103:13884–13889.

Stroop JR (1935): Studies of interference in serial verbal reactions. J Exp Psychol 18:643–662.

Swick D, Turken AU (2002): Dissociation between conflict detection and error monitoring in the human anterior cingulate cortex. Proc Natl Acad Sci USA 99:16354–16359.

Talairach J, Tournoux P (1988). Co-planar Steriotaxic Atlas of the Human Brain. New York: Thieme.

Taylor SF, Martis B, Fitzgerald KD, Welsh RC, Abelson JL, Liberzon I, Himle JA, Gehring WJ (2006): Medial frontal cortex activity and loss-related responses to errors. J Neurosci 26:4063–4070.

Ullsperger M, von Cramon DY (2001): Subprocesses of performance monitoring: A dissociation of error processing and response competition revealed by event-related fMRI and ERPs. Neuroimage 14:1387–1401.

van Veen V, Carter CS (2002): The anterior cingulate as a conflict monitor: fMRI and ERP studies. Physiol Behav 77:477–482.

van Veen V, Cohen JD, Botvinick MM, Stenger VA, Carter CS (2001): Anterior cingulate cortex, conflict monitoring, and levels of processing. Neuroimage 14:1302–1308.

van Veen V, Holroyd CB, Cohen JD, Stenger VA, Carter CS (2004): Errors without conflict: Implications for performance monitoring theories of anterior cingulate cortex. Brain Cogn 56:267–276.

Wittfoth M, Kustermann E, Fahle M, Herrmann M (2008): The influence of response conflict on error processing: Evidence from event-related fMRI. Brain Res 1194:118–129.

Yeung N, Botvinick MM, Cohen JD (2004): The neural basis of error detection: Conflict monitoring and the error-related negativity. Psychol Rev 111:931–959.